International Shipbuilding Progress 54 (2007) 25–44
IOS Press

Pressure and drag influences due to tunnels in high-speed planing craft

V. Anantha Subramanian *, P.V.V. Subramanyam and N. Sulficker Ali
Department of Ocean Engineering, Indian Institute of Technology Madras, Chennai 60036, India

Tunnels or 'propeller pockets' are often a necessity in planing crafts, in order to accommodate propellers and minimize the shaft angle. Computational Fluid Dynamics (CFD) is increasingly being used as a design tool for the purpose of modelling ship flows. This is due to advances in computational methods together with improvement in performance and affordability of computers. Qualitative information to decide the relative merits of aspects, such as flow alteration in and around the ship hull, can be usefully deduced from careful CFD based analysis. In this paper, work has been undertaken to assess the pressures and resistance characteristics of a single chine high speed planing hull. A relatively full sized tunnel has been introduced in the numerical model. Using $k - \varepsilon$ turbulence model in FLUENT, combining the predicted trim angle from equilibrium considerations and an iterative process, the stable equilibrium flow conditions have been modelled. The dynamic pressures have been evaluated and by integration, they have been matched with the total weight of the vessel. Single phase flow has been used to obtain the dynamic pressures in the underwater hull region. The numerical model predicts more favourable trim and qualitatively reduced resistance. Experiments conducted in a towing tank, using a model with and without the tunnel, confirm that by providing the tunnel there is improvement in the resistance by appreciable reduction. Pressure measurements confirm the validity of the numerical predictions obtained from CFD. It is quantitatively established that tunnels may be designed with beneficial effects for resistance.

Keywords: High speed planing craft, tunnels, resistance, extrapolation methods, pressure distribution, CFD studies

1. Introduction

In recent years Computational Fluid Dynamics (CFD) codes have been applied to modelling ship flows. The increased application is due to advances in computational methods together with the increase in performance and affordability of computers. The increased use of CFD has established the use of commercial CFD codes as credible design tools for solving practical flow problems such as the highly complex problem of flow past ship hulls. Today CFD does give qualitative information to decide the relative merits such as flow alteration in and around the ship hull due to the geometry of the tunnel.

*Corresponding author. Tel.: +91 44 22574812; E-mail: subru@iitm.ac.in.

Planing crafts are high-speed marine vehicles, with applications ranging from small pleasure boats to large military crafts. Generally in a properly configured planing hull form the deadrise angle diminishes from bow towards stern. High-speed planing crafts have hard chine, and may have both longitudinal and transverse steps at intermediate positions over the wetted region. The planing craft is typically run with a small bow-up trim or attack angle.

Because of the constant deadrise angle at the aft, planing crafts often have constraint of space for accommodating propellers. A solution to this problem is to provide propellers on inclined shafts. Another alternative is to provide tunnels (also called "propeller pockets") at the bottom of planing hulls. The enhancement achieved by using a partial tunnel includes reducing the shaft angle, decreasing navigational draft and allowing the propulsion machinery to be moved aft for an appropriate longitudinal centre of gravity location with improved arrangement of machinery space. By using tunnels, reduction of propeller diameter can be avoided. Therefore the provision of tunnels gives the designer freedom not to reduce propeller diameter and therefore efficiency. The question is how beneficial are tunnels, and if so, is there any trade offs in terms of other characteristics. In this work, numerical modelling has been undertaken to simulate the flow past the plain hull, and later with tunnels in the aft region.

2. Motivation

Quantitative analysis of tunnel influence is not evident in recent literature. Since the early 1960's several different planing hull forms have been systematically investigated for obtaining total resistance. Blount and Clement [2] presented a simplified prediction method for the estimation of planing hull resistance. Savitsky [12] presented a performance prediction method using the empirical equations for lift, drag, wetted area and centre of pressure. The method is still used as a first estimate method for planing hull resistance. Harbaugh and Blount [6] presented model resistance and self propulsion data from experiments modified for shallow and deep tunnels and with propellers of different diameters. They observed that the deep tunnelled hull in combination with propellers of large diameter and the smallest permissible tip clearance compare well performance-wise to the hull with no tunnels. Koelbel [8] studied the effect of tunnels and observed the changes in drag and propeller performance. Blount [1] provided guidelines for the design of partial propeller tunnels and relative placement of propellers to achieve exceptional vessel performance. Experimental and CFD studies have been carried out by Thornhill et al. [13] to measure the drag as well as pressure distribution on the planing vessel at steady speed through calm water. The lack of rigorous qualitative analysis of flow, pressure and resistance effects due to the presence of tunnels is the major motivation for the present study.

3. Methodology

3.1. Computational method for pressure and resistance

Simulation of flow around the hull has been performed by Computational Fluid Dynamics (CFD). The resistance and dynamic pressure acting on the surface of the hull have been obtained based on CFD solutions. The model equations governing the flow field and the solution strategy are discussed in the following sections.

3.2. Governing equations

The flow around the hull surface is governed by the incompressible form of the Navier–Stokes equation. The Reynolds-averaged form of the above momentum equation including the turbulent shear stresses is given by

$$\frac{\partial}{\partial t}(\rho u_i) + \frac{\partial}{\partial x_j}(\rho u_i u_j) = \frac{\partial}{\partial x_j}\left[\mu\left(\frac{\partial u_i}{\partial x_j} + \frac{\partial u_j}{\partial x_i}\right) - \left(\frac{2}{3}\mu\frac{\partial u_i}{\partial x_i}\right)\right] - \frac{\partial p}{\partial x_i} + \frac{\partial}{\partial x_j}\left(-\rho\overline{u_i' u_j'}\right),$$

where u_i' is the instantaneous velocity component ($i = 1, 2, 3$).

In order to characterise turbulence, additional conservation equations (or closure equations) for κ (kinetic turbulence energy) and ε (turbulence energy dissipation) are solved. In the present study, for closing the above set of equations Standard $k - \varepsilon$ model has been used since it is well established and the most validated turbulence model.

In the flow domain, the above RANS equation was solved using a SIMPLE (Semi-Implicit Method for Pressure Linked Equations) algorithm (Ferziger and Peric) [5] with STANDARD pressure correction [4]. The present CFD code employs a cell centered Finite Volume method that allows the use of computational elements with arbitrary polyhedral shape. Diffusion terms in the above equations are discretized with second-order central difference. Convective terms are discretized with first-order or second-order upwinding schemes and the local acceleration is solved using a first-order explicit scheme. Thus the RANS equation is first-order accurate in time and second-order accurate in space and the overall order of accuracy of truncation error is $O(\Delta t, \Delta x^2)$. Computations are performed with both first-order and second-order upwind schemes to assess the overall order of accuracy of the truncation error in the discretization of the convection terms.

Any numerical procedure should be validated with experimental results. The above numerical schemes have been extensively validated with experiments for the flow past under water bodies in the work of Jagadeesh and Murali [7].

3.3. Modeling and meshing

A high speed planing hull form of single hard chine type and designed for speed of 35 knots (corresponding to Froude number, Fn = 1.0 where Fn = $V/\sqrt{(gl)}$ was selected. The form is characterized by a fairly constant deadrise angle over the after half of the vessel. The details of the hull and the tunnels are shown in Tables 1 and 2. The body plan view is shown in Fig. 1.

The CAD model of the planing hull with and without tunnel created using the pre-processor is shown in Fig. 2. The planing hull model is fixed in the fluid domain using the trim and draft obtained from experiments. The fluid domain used for the

Table 1
Main particulars of the prototype

Particulars	Prototype
Length overall (LOA), m	37.8
Beam at transom (B_T), m	7
Beam max. at chines (B), m	7.1
Depth (D), m	5.36
B/T	4.7
L/B	4.68
Deadrise at transom (β_T), deg.	14
Deadrise at midsection (β), deg.	20
Design speed, knots	35
Model scale	20
Volume of displacement (∇), m^3	150/142*
Length on waterline (L), m	34.4/34.4
Wetted surface area (S), m^2	192/193*
LCG from transom, m	12.88/13.5*

*Values with and without tunnels at 1.5 m draught.

Table 2
Particulars of the tunnel

Particulars of tunnel	Prototype
Propeller immersion, %	33
A_T/A_P	0.12
L_T/L_P	0.319
Projected area, m^2	24.4
Length, m	11
Width at transom, m	1.3
Width near propeller region, m	1.46
Depth near propeller region, m	0.48

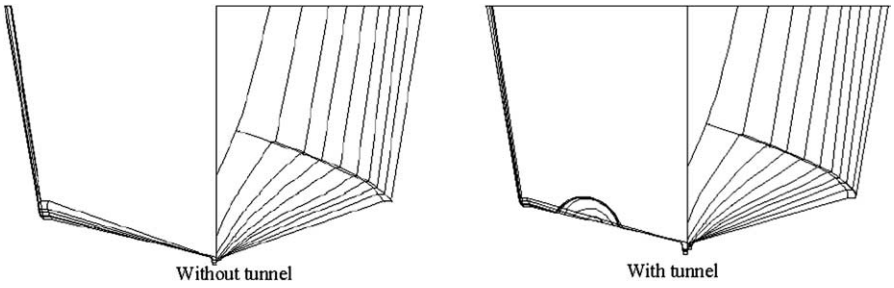

Fig. 1. Bodyplan of planing hull model without and with tunnel.

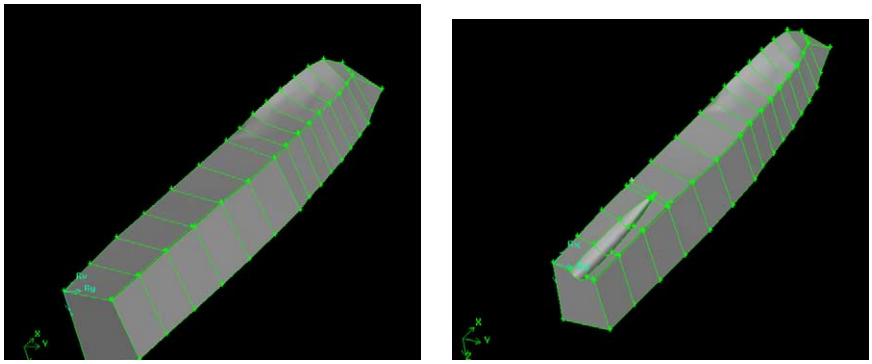

(a) (b)

Fig. 2. Planing hull models (a) without tunnel (b) with tunnel using pre-processor GAMBIT 2.0.

simulation is shown in Fig. 3 and the domain including the mesh with and without tunnel is shown in Fig. 4.

For the present study, which focuses on hull pressure distribution and primarily friction and viscous pressure drag of the planing hull, dense meshes were concentrated solely around the hull surfaces. The fluid domain was divided into three volumes for meshing. The first volume consists of the region closely surrounding the model surrounded by volume two and volume three. Unstructured tetrahedral elements have been used to discretized the domain since they have the flexibility to match with the surface of the complex geometries of the hull surface. The size of the element in each domain is decided based on the grid independence study. The size function has been used for meshing with the element size increased from 8 mm on the hull surface with a growth rate of 10% up to 25 mm at the outer surfaces in volume one. The volume two is meshed, starting with an element size of 25 mm at inner surface with a growth rate of 10% up to 40 mm at its outer surface. The volume three is meshed starting with an element size of 40 mm at inner surface with a growth rate of 10% up to 60 mm at the outer surface of the domain.

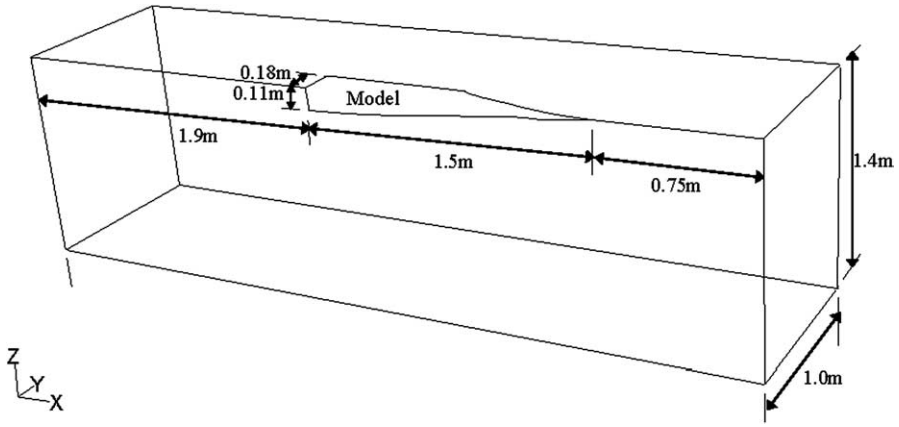

Fig. 3. Planing hull models flow domain.

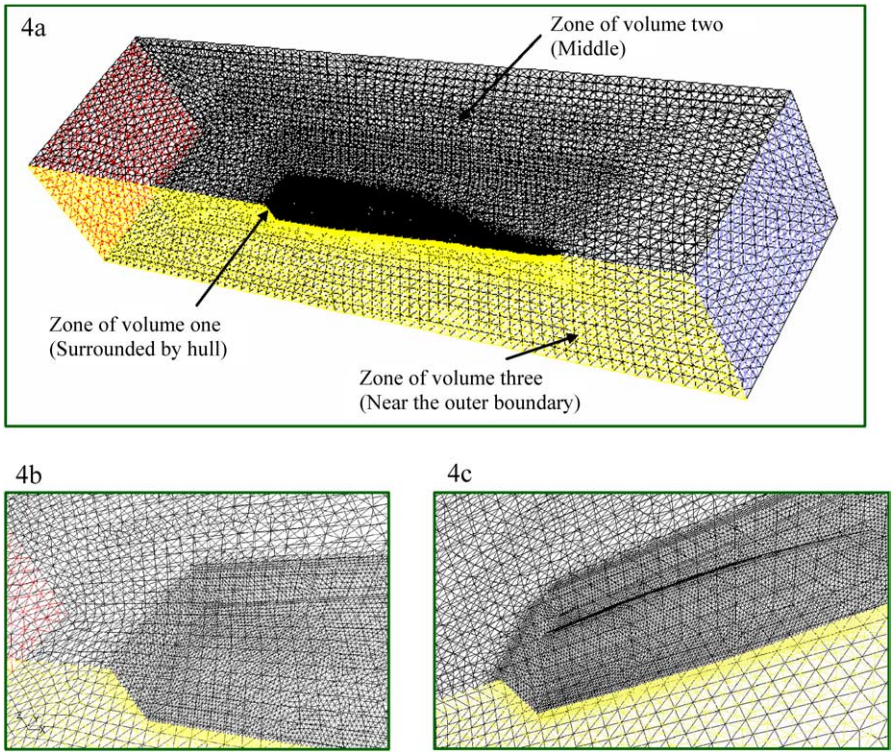

Fig. 4. (a) Domain with mesh and zoomed view near the aft region of the planing hull, (b) without tunnel (c) with tunnel.

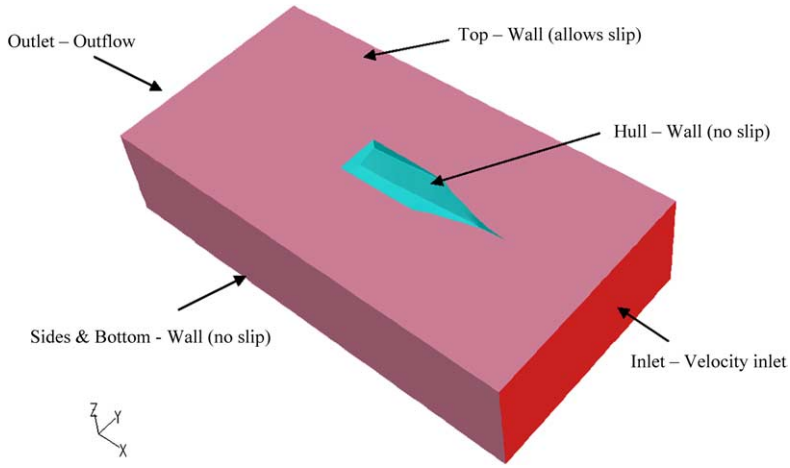

Fig. 5. Boundary conditions.

3.4. *Grid dependency study*

Grid independence studies were carried out by increasing the degree of fineness of the mesh in the domain to obtain optimum computational grid for accuracy. In the present study, the pressure distribution on the hull surface is used as a parameter for the grid dependent study. The computations are started with a coarse mesh of around 638,000 tetrahedral elements (25 mm on the hull surface) in the domain and the total pressure distribution along the vessel at 0.25B are plotted. Later the mesh in the domain is refined to see any variation in the pressure distribution. It can be seen from the total pressure plot that there is no further variation of the pressure distribution, when the mesh is refined from around 1,316,000 (8 mm on the hull surface) to 1,528,000 (5 mm on the hull surface) tetrahedral elements. i.e., the pressure predictions along the hull length have converged to nearly the same consistent values. For all further studies, the minimum cell size in the hull surface zone was selected to be of size 8 mm. This meshed domain and zoomed view of mesh near the aft region of planing hull model with and without tunnel is shown in Figs 4a to 4c. Figure 6 shows the results of the grid dependence studies.

3.5. *Numerical experiments*

All computations have been performed using the general purpose RANS solver FLUENT 6.0. All CFD studies performed here are based on model scale, in order to directly compare with the model based results. The computations are carried out over the relevant model speed range. Velocity inlet and outflow boundary conditions are used at the inlet and outlet of the domain. Symmetry boundary condition is applied at the central surface and a solid boundary condition with slip is enforced on the top of

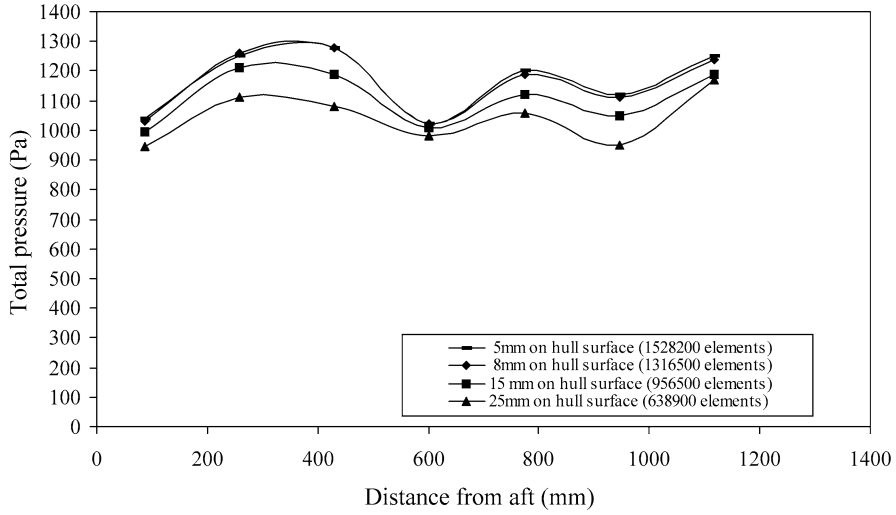

Fig. 6. Convergence criteria check using total pressure along the length of the planing hull model without tunnel (0.25B from centre line) for a model speed of 4.24 m/s ($\mathrm{Fn}_{\nabla} = 2.60$).

the domain and a solid wall with no slip condition is prescribed for the hull surface, side and bottom (see Fig. 5).

The computations were performed on a 64 bit processor SGI Origin 3800 Server (32 GB RAM). The processing time for a run containing about 0.6 million tetrahedral cells in the domain (coarse mesh, around 25 mm on the hull surface), using single processor was around 12 to 14 hours for achieving residual convergence requirement of 1×10^{-4}. The processing time for fine mesh (5 mm on the hull surface, 1.5 million elements in the domain) was around 24 to 26 hours.

Since the planing hull achieves dynamic lift and trim, both being unknowns, these have to be assessed first. The numerical modelling is updated on a 2 degree of freedom basis successively updating the trim and draught till the convergence criteria of weight equal to dynamic lift is obtained. The steady state trim and draught were obtained from the equilibrium condition following Savitsky [12] method described below, see Fig. 7.

The planing hull is said to be in equilibrium when it satisfies the following equation

$$\Delta\left\{\frac{[1-\sin\tau\sin(\tau+\varepsilon)]c}{\cos\tau} - f\sin\tau\right\} + D_f(a-f) = 0, \tag{1}$$

where

$$c = LCG - C_p\lambda b, \qquad a = VCG - (b/4)\tan\beta,$$

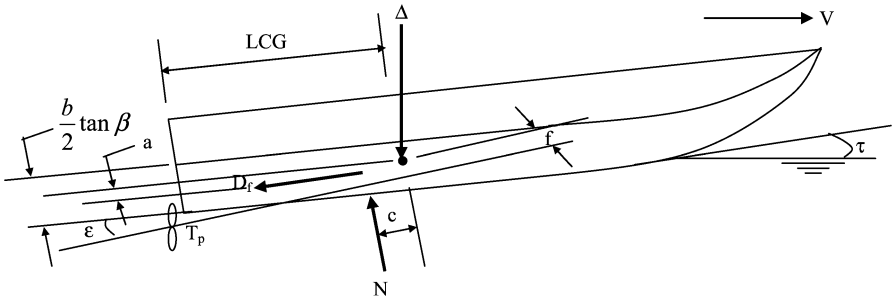

Fig. 7. Forces acting on the planing hull [12].

$$C_p = 0.75 - \frac{1}{5.21C_v^2/\lambda^2 + 2.39}, \qquad D_f = \frac{C_f \rho V_1^2 (\lambda b^2)}{2\cos\tau}.$$

$$\frac{0.242}{C_f} = \log_{10}(R_n C_f), \tag{2}$$

$$V_1 = V\left(1 - \frac{2p_d}{\rho V^2}\right)^{1/2}, \tag{3}$$

$$p_d = \frac{\Delta}{\lambda b^2 \cos\tau} = \frac{0.0120\tau^{1.1}V^2\rho}{2\lambda^{1/2}\cos\tau}. \tag{4}$$

It may be noted that the above scheme can only be iteratively used, ensuring that the first equation is satisfied by iterative choice of values of trim angle. Once the correct trim angle is obtained, the hydrodynamic drag is obtained from

$$D = \Delta\tan\tau + \frac{D_f}{\cos\tau}.$$

The trim angle in equilibrium condition with averaged draught condition was used to initiate the equilibrium check based on the computational scheme. Convergence was established when the vertical pressure integration matched the hull displacement. Using these initial trim and draught conditions the flow was simulated in FLUENT and iteratively the lift was obtained to match with the displacement.

Under the equilibrium condition of pressures and weight, the pressure contours are plotted as in Figs. 8 and 9. The enlarged views in Figs. 10, 11 show the bottom pressure distributions at $\mathrm{Fn}_\nabla = 1.86$ and 2.60 respectively. The pressures within the tunnel region are generally reduced due to the separation effect. In the overall underwater region near the hull, the pressures in the regions outside the tunnel (for the case of vessel with tunnel) are generally higher as seen in the contours.

Table 3

Iterative convergence of dynamic lift component to match displacement of vessel for a model speed of 4.24 m/s (all model scale) from FLUENT

Iteration	Trim angle (deg.)	Draught at transom (mm)	Lift (N)
With tunnel case (displacement = 178.6 N)			
1	3.5	112	160
2	4	112	202
3	4	108	192
4	3	108	176
Without tunnel case (displacement = 188.7 N)			
1	4	115	227.2
2	4	112	213.6
3	3.5	110	186.3

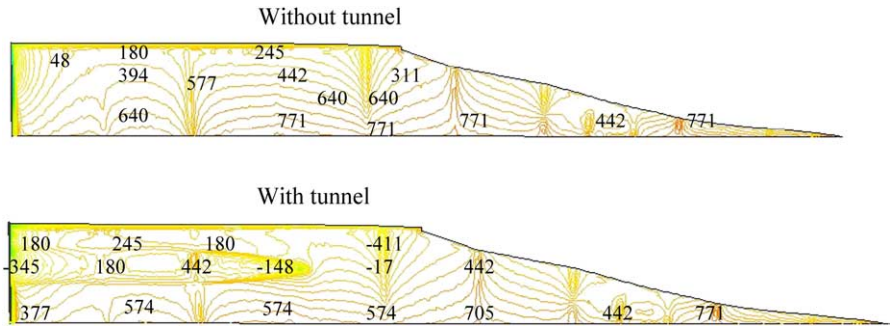

Fig. 8. Contours of total pressure (Pa) of planing hull model for model speed of 3.03 m/s (Fn = 0.74; Fn_{∇} = 1.86).

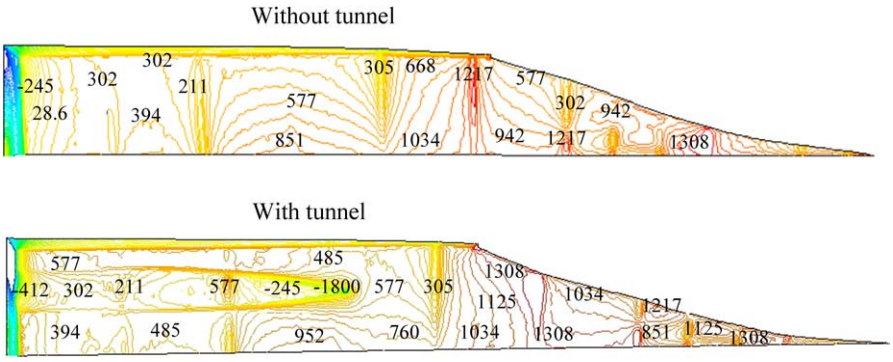

Fig. 9. Contours of total pressure (Pa) of planing hull model for model speed of 4.24 m/s (Fn = 1.03; Fn_{∇} = 2.60).

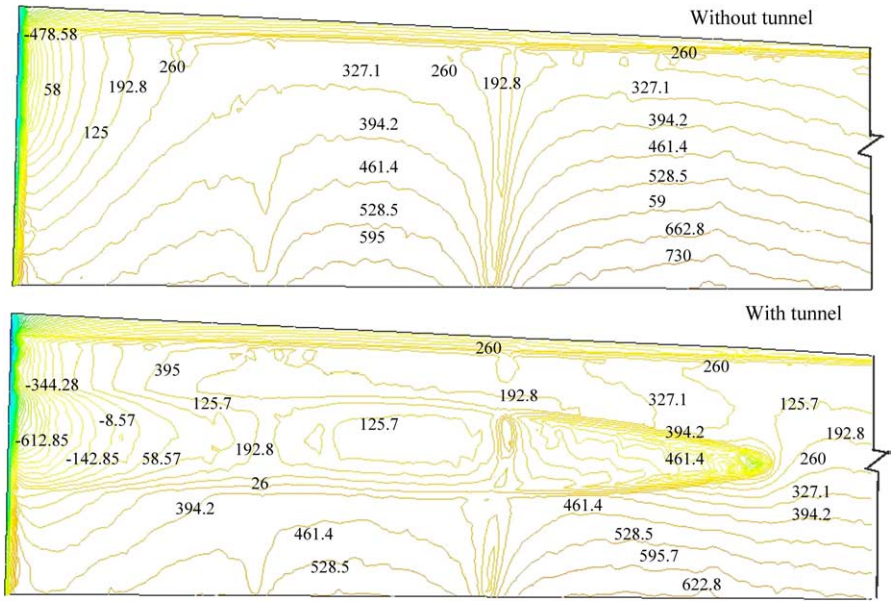

Fig. 10. Contours of total pressure (Pa) in the aft region of planing hull model for a model speed of 3.03 m/s (ship speed = 26.34 knots; Fn = 0.74; $Fn_{\nabla} = 1.86$).

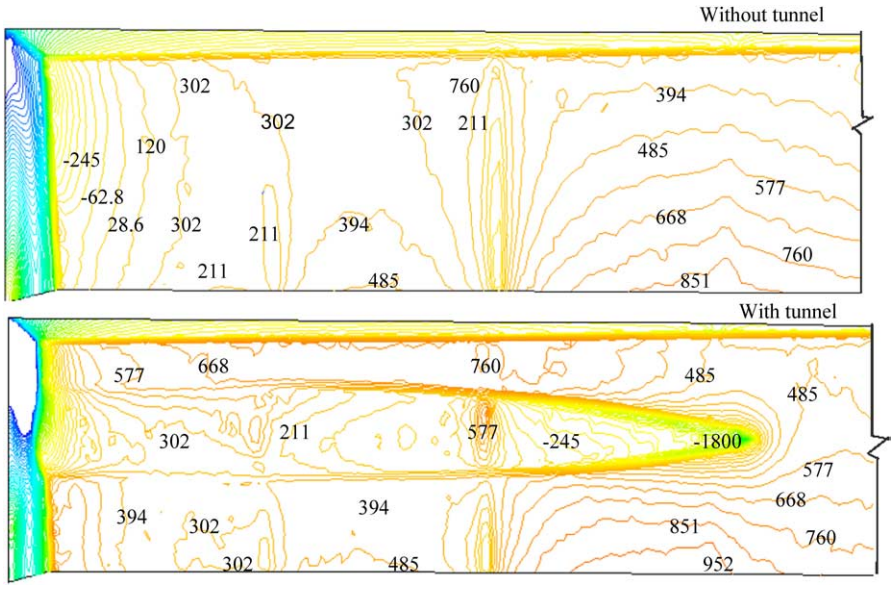

Fig. 11. Contours of total pressure (Pa) in the aft region of planing hull model for a model speed of 4.24 m/s (ship speed = 36.84 knots; Fn = 1.03; $Fn_{\nabla} = 2.60$).

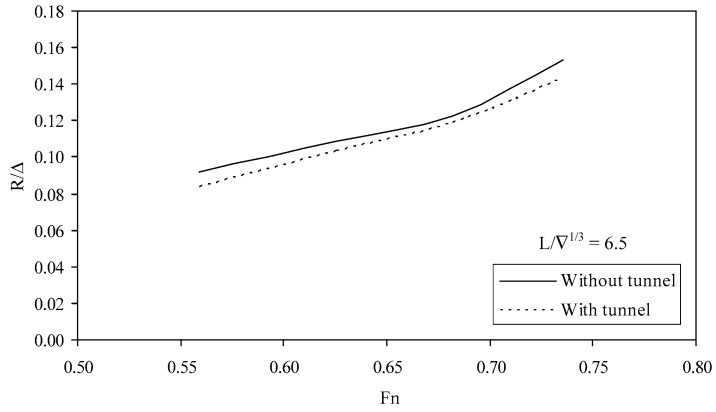

Fig. 12. CFD based comparison of resistance for planing hull with and without tunnel.

From the numerical study it is found that the region inside the tunnel is characterized by lower pressure because of separation. But just outside the tunnel the pressure is higher. The shift in the centre of pressure due to altered pressure conditions result in a more favourable trim condition for the hull with resultant favourable minimized resistance. The numerical resistance prediction is presented in Fig. 12. The numerical prediction clearly establishes a consistent reduced resistance for the case of hull form with tunnel.

Pressure measurements obtained from experiments have been used to compare with the numerical pressure predictions from the $k - \varepsilon$ turbulence model. For this purpose multiple pressure tappings were made and strain gauge based pressure transducers were used to instrument the model hull bottom. The pressures are compared at two different speeds and shown in Fig. 13. Within the limits of uncertainties, the experimental measurements can be read with 95% confidence.

The planing hull model at planing condition is shown in Fig. 14. The pressure tapping locations are shown in Fig. 15.

4. Experimental investigation

The experiments were performed to verify independently the magnitude of resistance in the case of with and without tunnel. For this purpose, the model was fabricated in glass-reinforced plastic (GRP) to a scale of 1:20. The model was modified with special bottom inserts which could be removed or filled to represent tunnel shape or 'no tunnel' condition respectively. The details of the hull and tunnels are shown in Tables 1 and 2. The body plan views are shown in Fig. 1. The tests were performed at three different draught conditions ($L/\nabla^{1/3}$ ratios of 6.8, 6.5 and 6.0 corresponding to draught of 1.3 m, 1.5 m and 1.7 m) to firmly establish the trend of drag component with and without tunnel influence. The model was designed with a

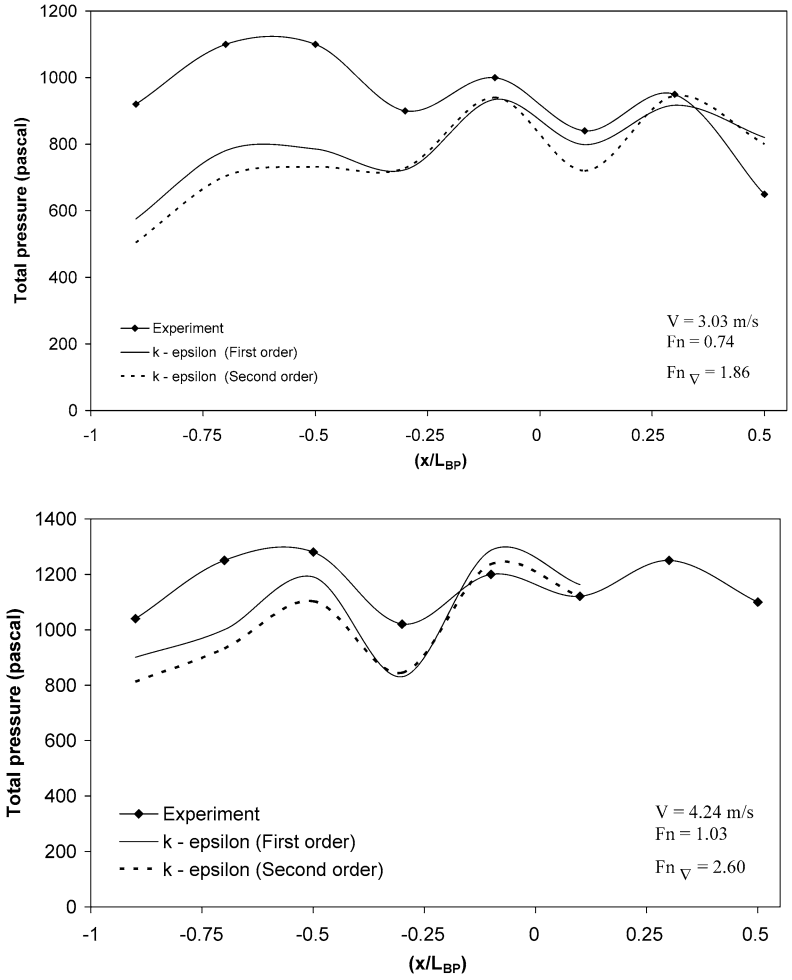

Fig. 13. Total pressure along the length of the planning model without tunnel, for $L/\nabla^{1/3} = 6.50$.

full featured tunnel with $A_t/A_p = 0.12$ (i.e., tunnel area ratio which is defined as projected area of tunnels to projected water plane area of hull). The towing experiments were carried out in a tank of dimensions 82 m $\times$ 3.2 m $\times$ 2.8 m at IIT Madras, India.

4.1. Uncertainty analysis for surface pressure measurement

The Uncertainty Analysis (UA) methodology and procedures adopted here are based on the 95% confidence, large-sample UA approach, recommended by the AIAA and ASME (Longo et al., 2005). Coleman and Steele (1995) have provided

Fig. 14. Planing hull model in towing test condition.

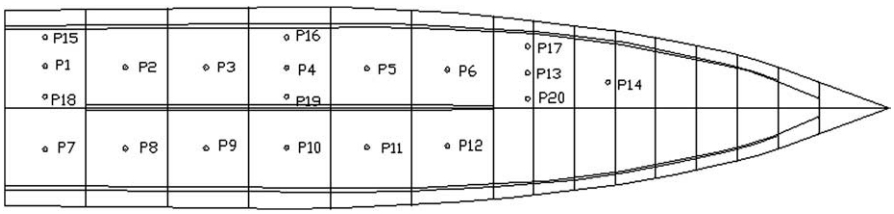

Fig. 15. Location of pressure tappings in planing hull model.

derivation and discussion of the overall methodology and procedure for uncertainty analysis. Total uncertainty is estimated with a root sum square (RSS) and normalization with the average value of the measured total pressure. Denoting the pressure related values with a subscript x, the total uncertainty is given by

$$U_x^2 = B_x^2 + P_x^2,$$

where

U_x is the uncertainty
B_x is the bias error
P_x is the precision error.

Bias error is the systematic component of the errors such as the calibration of the different elements of the measurement system or the sep-up of the system. For single

Table 4
Uncertainty analysis for total pressure measurement at $x/L_{BP} = 0.25B$ from the center line of the vessel

Magnitude of measured pressure (Pa)	Bias error (Pa)	Precision error (Pa)	Total uncertainty (%)
900	±20.41	6.47	2.3

and multiple tests, the bias limit of the result is given by

$$B_x^2 = \sum_{i=1}^{j} \theta_i^2 B_i^2,$$

where $\theta_i = \frac{\partial x}{\partial X_i}$ are the sensitivity coefficients and B_i is the bias limit in X_i.

An error is classified as a precision error if it contributes to the scatter of the data. They come from the repetition of the tests in the same conditions.

The precision error is given by

$$P_x = \frac{kS_x}{\sqrt{M}},$$

where

- k is the coverage factor and equals 2 from *t*-distribution, for a 95% confidence interval and large sample size
- S_x is the standard deviation of "x"
- M is the number of readings for the determination of "x".

Repeated measurements of total pressure were performed with ten runs and a coverage factor of $k = 2$ were used for calculating the precision error. The bias limit, precision limit and comprehensive uncertainty with a 95% confidence level are shown in Table 4.

5. Results and discussion

5.1. Pressure measurements and comparison

The objective of pressure measurements was to obtain the distribution of pressure in the planing condition and to validate CFD based measurements by comparison. For this purpose the pressure measurements were confined to the case of without tunnel. The pressure plot as measured at each location and as a function of speed is given in Fig. 16. The pressures measured at the forward most point of contact with water i.e., the spray root region, shows the highest growth of pressure with speed. This pressure vs. velocity curve has the highest gradient. After the transition to full planing mode, the pressures are concentrated maximum at the spray root region and are high at the mid-aft region. Further towards aft, the pressures diminish.

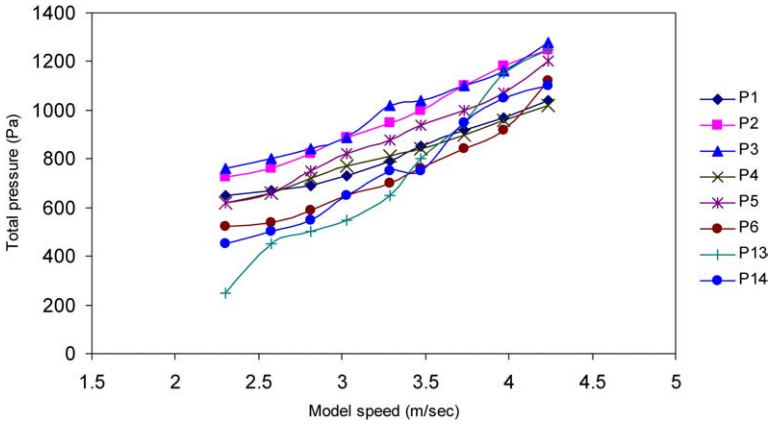

Fig. 16. Total pressure for various model speeds at different pressure tapping locations.

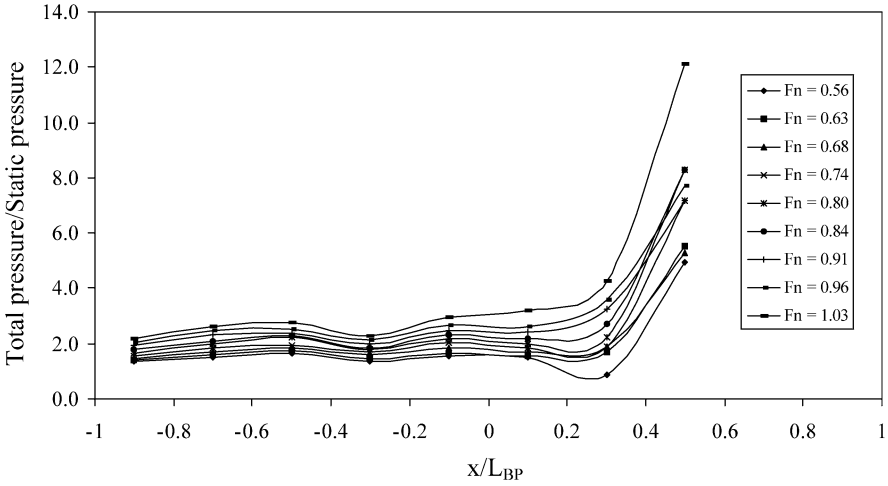

Fig. 17. Non-dimensional pressure along the length of the planing hull model without tunnel.

The spatial pressure distribution is shown in Fig. 17. The graph shows the consistent concentration of pressure at the spray root region and the growth of pressure as a function of Froude number and the sharp fall of pressure behind the spray root region. At regions behind it, the average pressures are nearly constant. The pressure measurements provide inputs for dynamic pressure distributions required for hull design under planing condition.

5.2. Resistance results

The measured trim and CG changes of the model (T = 1.5 m, $L/\nabla^{1/3} = 6.5$) due to the effect of the tunnel are shown in Figs 18 and 19. At full planing speed ($F_{n\nabla} > 1.5$) the trim is more for the case of the vessel without tunnel. It is obvious that with the present tunnel ($A_T/A_P = 0.12$) the flow for the aft is favourably modified to give the ship a reduced (favourable) trim condition. Similarly the centre of gravity rise is reduced in the case of the vessel with tunnel. There is the characteristic drop of centre of gravity in both cases (i.e. with and without tunnel) at pre-planing speeds.

The non-dimensionalized resistance plots are shown in Fig. 20. The modified Froude's extrapolation method accounting for modified velocity conditions under the model has been used for obtaining the resistance. When tested with tunnel, the consistent reduction of resistance at all the three draught conditions is evident. CFD results follow a similar trend.

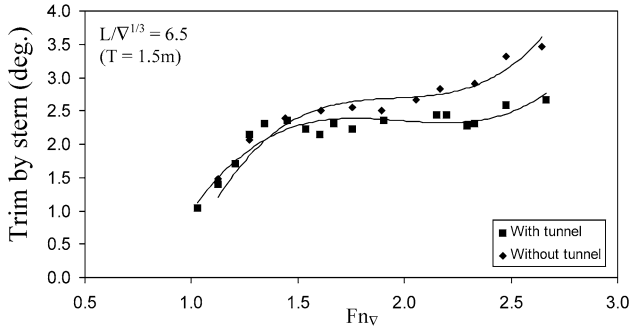

Fig. 18. Trim changes with respect to speed.

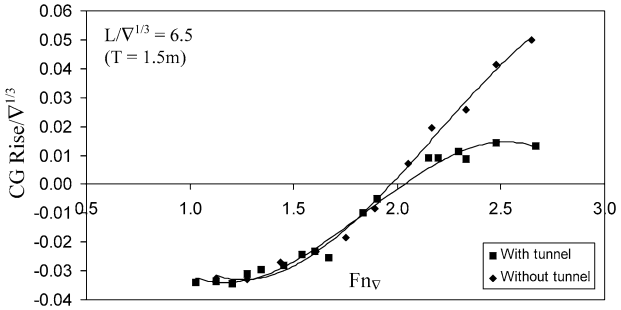

Fig. 19. CG rise with respect to speed.

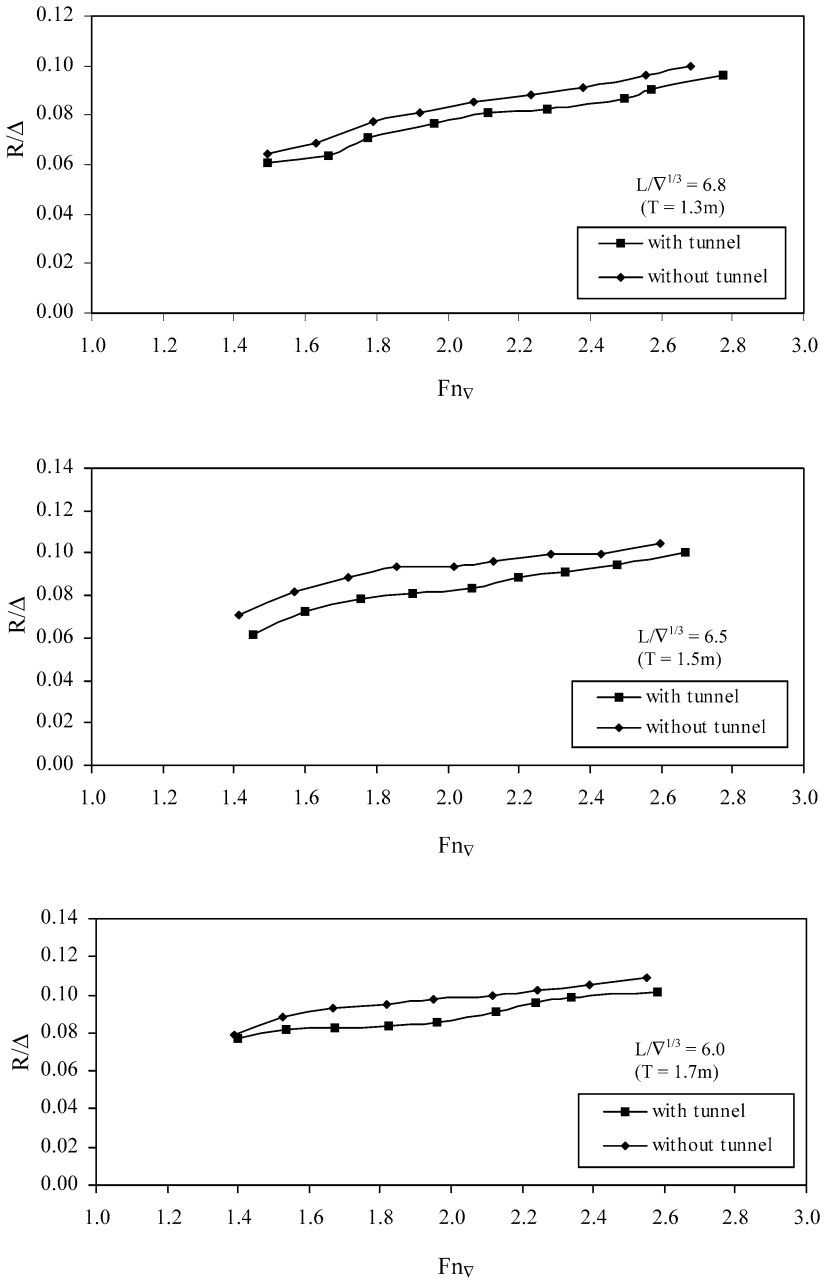

Fig. 20. Resistance with and without tunnels at different draughts (modified Froude extrapolation method).

6. Conclusion

The $k - \varepsilon$ turbulence model based prediction has characterized the effect due to the tunnel in the case of a high speed planing hull. The pressure distributions around the tunnel region are modified and the overall result is to make the resistance more favourable. The experiments in resistance measurement have confirmed the favourable resistance characteristics of the hull form with tunnel. The pressure measurements conducted separately also confirm the trend of predictions in the turbulence model. The typical peak pressures in the spray root region are also brought out. The use of CFD for analysis and improvement of flow past the hull with tunnels is demonstrated.

Nomenclature:

a	Distance between D_f and CG
A_P	Projected area of the planing hull
A_T	Projected area of the tunnels
b	Beam
B	Beam
c	Distance between centre of pressure and LCG
C_f	Schoenherr turbulent friction coefficient
C_p	Centre of pressure
C_v	Coefficient of velocity
CFE	Conventional Froude extrapolation
CG	Centre of gravity
d	Draft of keel at transom
D	Total drag
D_f	Viscous component of drag
f	Distance between T and CG
Fn	Froude number
Fn_∇	Volume based Froude number
k	Turbulent kinetic energy
L	Length on waterline
L_{BP}	Length between perpendiculars
LCG	Longitudinal centre of gravity
MFE	Modified Froude extrapolation
N	Resultant of pressure forces acting normal to bottom
P1 to P14	Pressure transducer locations from 1 to 14
R_n	Reynold's number
T	Draught
T_p	Propeller thrust
V	Forward speed

V_1	Average bottom velocity
VCG	Vertical centre of gravity
x	Distance of pressure tapping location measured from transom
β	Deadrise angle
∇	Volume of displacement
Δ	Displacement
ε	Turbulent energy dissipation rate
λ	Wetted length to beam ratio
ρ	Mass density of water
τ	Trim angle

References

[1] D.L. Blount, Design of propeller tunnels of high-speed craft, in: *FAST'97*, Sydney, Australia 1997.

[2] D.L. Blount and E.P. Clement, Resistance tests of a systematic series of planing hull forms, *SNAME Transactions* (1963), 491–579.

[3] H.W. Coleman and G.W. Steele, *Engineering Application of Experimental Uncertainty Analysis*, John Wiley Publication, 1995.

[4] Fluent6.0 User's Manual, Copyright Fluent Incorporated, 2004.

[5] H. Ferziger and M. Peric, *Computational Methods for Fluid Dynamics*, Springer, 2002.

[6] K.H. Harbaugh and D.L. Blount, An Experimental Study of a High Performance Tunnel Hull Craft, SNAME Spring Meeting, Lake Buena Vista, FL (1973).

[7] P. Jagadeesh and K. Murali, Verification and validation of CFD simulations past axisymmetric underwater bodies, *Journal of Naval Architecture and Marine Engineering* **2**(1) (2005).

[8] J.G. Koelbel Jr., *Tunnel Hull Designs for U.S. Navy Small Craft*, Combatant Craft Engineering, Naval Ship Engineering Center, Norfolk Division, 1979.

[9] K. Kume, Y. Ukon and J. Fujisawa, Uncertainty analysis for KCS model tests in the SRI 400 m towing tank, Ship Research Institute, Japan, 2000.

[10] J. Longo and F. Stern, Uncertainty assesment for towing tank tests with example for surface combatant model 5415, *Journal of Ship Research* **49**(1), 2005.

[11] L.P. Rojas, J.V. Cabezas and A.S. Iglesias, The future in experimental ship hydrodynamics, Canal de Experiencias Hidrodinámicas de El Pardo, Spain.

[12] D. Savitsky, Hydrodynamic design of planing hulls, *Marine Technology* **1**(1) (1964), 71–95.

[13] E. Thornhill, N. Bose, B. Veitch and P. Liu, Planing hull performance evaluation using a general purpose CFD code, in: *Proceedings of 24th Symposium on Naval Hydrodynamics*, 2003.